# Pool Boiling of Novec 7300 and DI water on Nano-textured Heater Covered with Supersonically Blown or Electrospun Polymer Nanofibers

Sumit Sinha-Ray[a], Wenshuo Zhang[a], Rakesh P. Sahu[a], Suman Sinha-Ray[a,b,c], Alexander L. Yarin[a]

[a] Department of Mechanical and Industrial Engineering, University of Illinois at Chicago, Chicago, Illinois 60607-7022, USA

[b] Corporate Innovation Center, United States Gypsum, 700 US 45 N, Libertyville, IL-60048

[c] Department of Materials Science and Engineering, Indian Institute of Technology, Indore, Madhya Pradesh 452017, India

## Abstract

In this work we study pool boiling of Novec 7300 and DI water on bare copper surface and copper surface covered with supersonically-blown or electrospun polymer nanofibers. In distinction from the previous works nanofibers were not metal-plated. The elimination of the electroplating makes nano-texturing process extremely simple and applicable to a wide variety of surfaces. On the other hand, it comes with the price of a lower heat removal rate compared to that on metal-plated nanofibers, albeit the present experiments revealed that the reduction is not that drastic as it would be expected. It is
* Correspondence should be addressed to E-mail: ayarin@uic.edu. Phone: +1(312) 996-3472. Fax: +1(312) 413-0447.

.

also demonstrated that the supersonically-blown polymer nanofibers also outperformed the electrospun nanofiber-coated surface. Supersonically-blown nanofibers provide a large number of nucleation sites than electrospun nanofibers or bare copper surface, and thus, facilitate nucleate boiling much stronger. The ultrafine supersonically-blown polymer nanofibers are very robust and did not delaminate from the heater surface either in Novec 7300 or DI water after prolonged vigorous boiling process. Overall, the enhancement of heat removal due to the ultrafine supersonically-blown polymer nanofibers on the heater surface in Novec 7300 is more significant than in DI water, which is associated with the smaller bubble size in the former case.

## 1. Introduction

Ever growing need of miniaturization of transistors in microelectronic components aimed to increase computational speed, facilitate automation, data processing, etc., has posed severe challenges in terms of heat dissipation and an effective heat removal. For smaller transistors, densely crowded in integrated circuits, thermal management becomes critical to avoid thermal failure due to differential thermal expansion of components and extend their operational lifetime [1,2]. Several approaches to cooling microelectronics were explored in the past, such as single-phase liquid cooling [3-5], flow boiling [6,7], jet impingement cooling [8-10], spray cooling [11], heat pipes [12], liquid metal cooling [13,14], indirect cooling with phase change materials [15], and pool boiling [16, 17]. Pool boiling is one of the most promising methods of thermal management problem, which stems from high latent heat of evaporation of liquids. Pool

boiling is relevant for thermal management of nuclear power plants, refrigeration, metallurgical quenching processes, petrochemical processes, and air conditioning. In the latter, different refrigerants are used which release heat at the evaporators in refrigeration system in the so-called flooded regime with pool or flow boiling at solid surfaces. Heat removal in pool boiling steeply rises when nucleate boiling sets in due to convective heat transfer by buoyant bubbles, albeit it begins to decrease steeply as the Critical Heat Flux (CHF) is reached and a subsequent film boiling sets in [18].

Surface modification can significantly enhance the bubble nucleation process and thus facilitate pool boiling [19]. The macroscopic shape and features of the heater surface, e.g. a wire or a plane surface, rough or smooth surface, an intact or porous one, a wettable or a non-wettable surface also matter [20-30].

Heat removal in pool boiling significantly depends on the coolants used, and such coolants as DI water, alcohols, Fluorinert fluids and fluid mixtures were explored [31-38]. Suspensions of nanoparticles [39-41] or surfactant solutions [42] were also used as coolants aiming to shift the CHF to a higher value.

Electrospun polymer nanofiber mats deposited on a heater surface create a nano-textured porous interface which facilitates pinning of the impacting coolant drops on the surface, which dramatically enhances heat removal rate and even eliminates the Leidenfrost effect [43]. Nano-textured surfaces formed using metal-plated electrospun nanofiber mats were used to enhance heat removal rate in spray cooling [44-46] and pool boiling [47]. These inexpensive nano-textured surfaces allowed achieving heat removal rates close to 1 $kW/cm^2$ in drop impact cooling [44]. In the case of pool boiling the rough

metal-plated nanofibers act as nucleation sites, as well as a hot “cage” for growing bubbles, i.e. simultaneously increase the number of bubbles and their growth rate [47].

Nanofibers even smaller than the electrospun ones were recently developed using a novel method of supersonic solution blowing [48]. These nanofibers, being metal-plated, revealed a much better robustness than their electrospun counterparts and could withstand delamination from the heater surface even after multi-hour vigorous pool boiling [49]. They also removed higher heat fluxes at lower surface superheats, and were able to delay the onset of CHF [49, 50].

Supersonically-blown nanofibers were used so far for the enhancement of heat transfer in pool boiling only in metal-plated form. Metal-plating of fibers on heater surface is not only an extra fabrication step but also might be dangerous for certain microelectronics substrates. Therefore, it would be attractive to eliminate metal-plating, if it would be possible to sustain a certain level of heat enhancement. It was recently shown that supersonically-blown polymer nanofibers not only enhance heat transfer and lower surface superheat in mini-channel flows with Taylor bubbles but also sustain adhesion to the heater surface for a long time [51]. Therefore, in the present work pool boiling of Novec 7300 fluid and DI water are studied on bare copper surface and nano-textured surface covered with polymer, non-metallized electrospun and supersonically-blown nanofibers. Section 2 describes the experimental details. The experimental results are presented and discussed in section 3, and conclusions are drawn in section 4.

## 2. Experiments

### *2.1 Materials*

Polymer, polyacrylonitrile (PAN; molecular weight $M_w$=200 kDa) was obtained from Polymer Inc. Solvent for PAN, N,N-Dimethyl formamide (DMF) anhydrous-99.8%, was obtained from Sigma-Aldrich. Novec 7300 engineered fluid was purchased from 3M. Also, DI water was used. Oxygen-free high-conductive (OFHC) 101 grade copper rods purchased from Mcmaster-Carr were used as a heated substrate. These copper rods were cut into cylindrical pieces as disks of 1.9 cm in diameter and 1.9 cm in height. The surfaces of these substrates were smoothened using 3M 2000 Grit sandpaper and are denoted hereinafter as bare copper surfaces. In addition, smoothened copper surfaces with deposited polymer nanofibers were also used as heaters and are denoted hereinafter as nano-textured heater surfaces.

### *2.2 Electrospinning and Supersonic Solution Blowing*

Electrospinning of PAN was carried out in the following order. First, 9 wt% PAN solution in DMF was pumped through a 5 mL syringe with a 20G needle connected to it. A syringe pump, purchased from New Era Pump Systems, was employed for pumping the solution at 0.6 mL/h. The Cu substrate was grounded, while the needle was the positive electrode. Electrospinning was carried out at 9 kV with the tip-to-collector distance being 25 cm. Electrospun fibers were collected for 45 s. The electrically-assisted supersonic solution blowing was carried out using 6 wt% PAN solution as described by the present group elsewhere [48, 49]. The solution flow rate was 0.1 mL/h. Copper

cylinders were used as the substrates located at a distance of 37.5 cm from the supersonic nozzle. Nanofibers were collected for 4 min.

The total amount of nanofibers deposited on the samples is difficult to accurately measure directly, since the nanofiber mass is significantly smaller than that of the substrate. However, the nanofiber mass can be controlled by controlling the total deposition time, which was kept constant. Electrospun nanofibers were collected for 45 s and the supersonically blown nanofibers were collected for 4 min. For electrospinning, the PAN solution concentration was 9 wt%, while the flow rate was maintained at 0.6 mL/h, which means that approximately 0.68 mg of polymer nanofibers were deposited (taking the polymer solution density of 1 $g/cm^3$). Similarly, for supersonic blowing the mass of the deposited polymer nanofibers was approximately 0.4 mg. Accordingly, the mass of the deposited polymer nanofibers was similar in both the processes. However, it should be emphasized that due to the fact that the area of the sample covered by nanofibers was small in comparison to the overall area over which the nanofibers are normally deposited, only a small fraction of the above mentioned mass was deposited onto the samples used in the boiling experiments. Still, it was almost the same for both processes and samples.

### *2.3 Nanofiber Characterization*

Scanning electron microscopy (SEM) of nanofiber mats employed JEOL JSM-6320F (Research Resource Center, RRC UIC) with a cold emission source.

### *2.4 Pool Boiling Setup*

The experimental setup employed in the present investigation was described by this group elsewhere [50]. In brief, it consists of (i) two layers of teflon casing for proper thermal insulation; (ii) the main copper cylinder with five cartridge heaters (200 W), purchased from Omega, inserted into it for uniform heat supply to the Cu substrate separately screwed on it; (iii) the glass chamber containing the working liquid; (iv) the recuperation unit to facilitate vapor condensation and returning back to the liquid pool. The schematic of the experimental setup is shown in Fig. 1. The main Cu substrate, to be tested, was of 1.9 cm of diameter and 1.9 cm in height. It was screwed to the primary copper rod of length 7.6 cm. Before screwing the substrate to the main cylinder, a thin layer of thermally conductive silver paste (obtained from MG Chemicals Inc.) was applied between the substrate and the cylinder. The main cylinder was machined from a diameter of 4.44 cm to 1.9 cm for proper intensification of the heat flux supplied from the above-mentioned heaters inserted into it. The primary teflon case containing the Cu cylinder had an insulating air gap of 0.6 cm between teflon and the Cu cylinder. Using teflon as a casing for the entire heating chamber was appropriate for the outer thermal insulation. Two holes were drilled laterally within the copper substrate at a distance of 0.625 cm between them. The holes were drilled to the center of the copper substrate to allow thermocouples to be put through them. A small amount of silver paste was also applied on the thermocouples for proper contact with the copper substrate and accurate temperature reading. These two T-type thermocouples were plugged to a HH806AW thermometer (Omega). The secondary teflon casing was attached to the glass chamber, the outer casing of which was made of aluminum. The boiling chamber was of the sizes

3.81 cm × 3.81 cm × 8.26 cm. The teflon assembly was then placed surrounding the Cu substrate and exposing the substrate to the liquid that would fill the boiling chamber. An O-ring was used inside teflon to seal the gap between the copper substrate and the secondary teflon casing. The vapor recuperation unit made of Aluminum was then placed on top of the boiling chamber. The unit contained multiple channels drilled through it to circulate cold DI water and to keep the temperature of the unit below room temperature and facilitate vapor condensation. This allowed sufficient cooling at the top of the chamber and kept a steady vertical temperature gradient during the boiling experiments. A small hole of 0.1 cm in diameter was drilled at the top of the recuperation unit which allowed the excess vapor formed inside the chamber to escape out to avoid any pressure rise inside the chamber. A 100 W immersion heater (obtained from Watlow) was inserted into the boiling chamber to keep the temperature of the liquid close to the saturation conditions during the entire experiment and also to degasify the liquid as much as possible. Both the immersion heater and the cartridge heater assembly were then connected to two separate variable transformers for controlling the heat input.

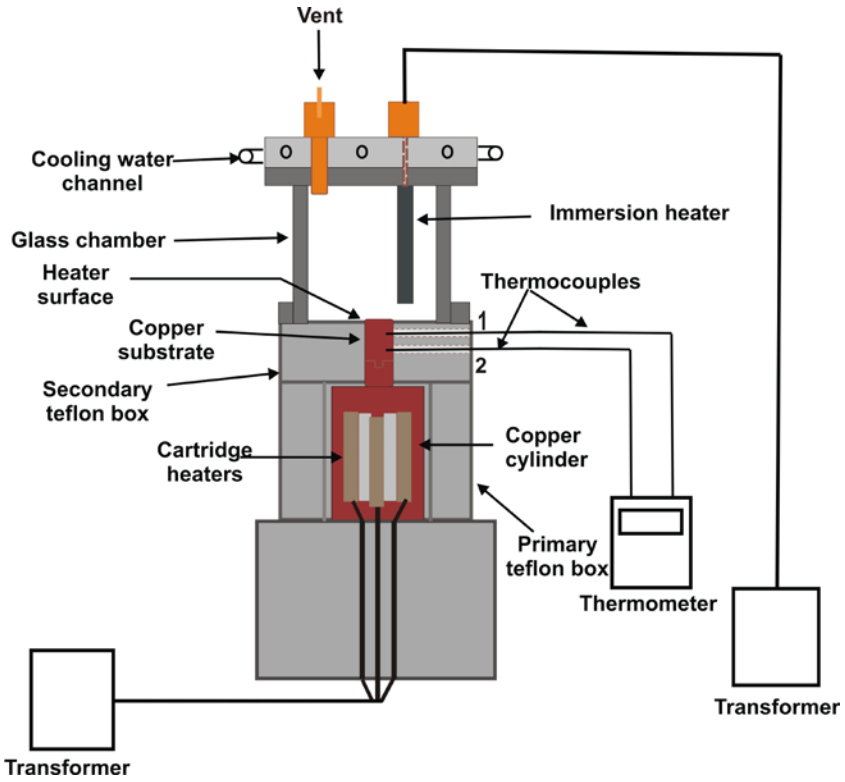


**Fig. 1.** Sketch of cross-sectional view of the assembled experimental setup used for the pool boiling experiments.

### *2.5 Pool Boiling Experiments*

Pool boiling experiments were carried out using two different liquids: DI water and Novec 7300 engineered fluid (3M). Three types of the heater surfaces were used in these experiments: bare Cu surface (denoted as Bare), Cu surface with electrospun polymer nanofibers on top of it (denoted as Bare+E), and Cu surface with supersonically-blown polymer nanofibers on top of it (denoted as Bare+SB). During each experiment, 90 mL of liquid was used. The immersion heater was operated at 120 V of transformer output (100%) the entire duration of any experiment. The cartridge heater assembly was,

however, operated differently in different experiments. For DI water, initially the cartridge heaters were operated at 18% of transformer output and kept at this output for approximately 50 min until the two thermocouples would record a steady-state temperature; after that the transformer was turned to 20% output. After 10 min at this setting as the two temperature records would become steady again, the temperatures were recorded. After that, the output was raised by 4% and kept for 10 min until steady-state temperatures would be recorded. At the end of this ramp, the final transformer output was kept at 60% for all the experiments with DI water, since beyond that the heat flux would have reached CHF and a vigorous temperature rise began.

For Novec 7300 fluid, in all the cases the initial transformer output was at 16%. The further rise in transformer output was kept by 2% after 10-12 min until the temperature records become steady again, while the final output at the end of this ramp was limited to 34% before CHF could be reached. During the entire boiling experiments with NOVEC 7300 fluid, the immersion heater was used to keep liquid at saturation temperature and to achieve as much degasification as possible prior to the boiling onset (for 50 min).

## 3. Results and Discussion

### *3.1 General Definitions*

Pool boiling experiments on copper substrate, with or without polymer nanofibers, were conducted using two different liquids, DI water and Novec 7300 fluid, as two limiting cases. Though their boiling points are close (98 $^{0}$C for Novec 7300 fluid

and 100 $^0$C for DI water) they differ markedly in terms of their specific heat capacity, 1.14 kJ/kg-K for Novec 7300 fluid and 4.2 kJ/kg-K for DI water, their surface tension, 15 mN/m for Novec 7300 fluid and 72 mN/m for DI water, and their latent heat of evaporation 102 kJ/kg for Novec 7300 and 2257 kJ/kg for DI water. In previous works of this group it was shown that copper-plated electrospun and supersonically-blown nanofibers significantly enhance heat removal rate in nucleation boiling regime at low surface superheat for both Novec 7300 and DI water, and also for such low surface tension liquids as, for example, ethanol (20 mN/m) [49,50]. The present work aims to explore to what extent the positive effect of copper-plated nanofibers could be retained with pure polymer (not copper-plated) nanofibers, even though the surface textures of individual nanofibers of these two types are drastically different and the thermal conductivity of the former is significantly higher than for the latter ($k_{Cu}$= 401 W/m-K versus $k_{PAN}$= 0.26 W/m-K, respectively). The main aim of the present experiments is to explore the structural integrity (robustness) of pure polymer nanofibers in nucleate boiling and their capability to enhance heat removal rates.

The thermocouples 1 and 2 in Fig. 1 measured, respectively, temperatures $T_1$ and $T_2$ which were used to determine the surface temperature of the substrate $T_s$ as

$$T_s = T_1 - \left( \frac{T_2 - T_1}{\Delta x_{12}} \right) \Delta x_{1s} \tag{1}$$

where $\Delta x_{12}$ is the distance between the locations of thermocouples 1 and 2, and $\Delta x_{1s}$ is the distance between the location of thermocouple 1 and the top surface exposed to

liquid. Equation (1) is determined by the linearity of the practically one-dimensional temperature distribution along the copper substrate.

Accordingly, the degree of superheat $\Delta T = T_s - T_f$, where $T_f$ is the saturation temperature of the boiling liquid. The heat transfer to the boiling liquid from the substrate surface is found using the Fourier law as

$$q'' = k_{Cu}\left(\frac{T_2 - T_1}{\Delta x_{12}}\right) \quad (2)$$

### *3.2 Pool Boiling of Novec 7300 Fluid*

All experiments were conducted thrice for the same sample. For Novec 7300 fluid nucleation of vapor bubbles was observed at the Bare+SB surface at $\Delta T$ lower by 1 $^0$C than on Bare or Bare+E surfaces. Accordingly, the pool boiling curve is shifted toward lower surface superheat on Bare+SB surface than on either Bare or Bare+E surfaces, cf. Fig. 2a. The corresponding heat transfer coefficient h=q"/ $\Delta T$ is shown in Fig. 2b.

Not only supersonically-blown polymer nanofibers revealed higher heat removal rates at the same surface superheat and thus outperformed the bare surface and the surface covered with electrospun polymer nanofibers, they also revealed the pool boiling enhancement quite comparable to that of copper-plated supersonically-blown nanofibers in [50]; cf. Fig. 2c. The latter is quite amazing, since copper plating not only introduces additional nucleation sites (the copper-plated thorny-devil nanofibers of [50] are very rough compared to the relatively smooth polymer nanofibers of the present work) but also increases thermal conductivity of the nanofiber mat. Still, copper-plated

supersonically solution-blown nanofibers outperform the non-plated ones, as Fig. 2c shows. Namely, the difference in the heat fluxes between them at the same surface superheats is quite significant. After the surface superheat of about 7.5 ºC copper-plated nanofiber mat outperforms the non-plated nanofiber mat. At the surface superheat of about 10 ºC copper-plated thorny devil nanofibers remove about 44% more heat in comparison to the non-plated ones. In fact, Fig. 2c clearly shows that an additional nano-texture associated with metal nucleation sites created by copper-plating are beneficial for heat removal. Still the non-plated supersonically-blown pure polymer nanofibers yield significant benefits too compared to the bare surface or to the larger electrospun nanofibers, which is ascertained by the results shown in Figs. 2a and 2c.

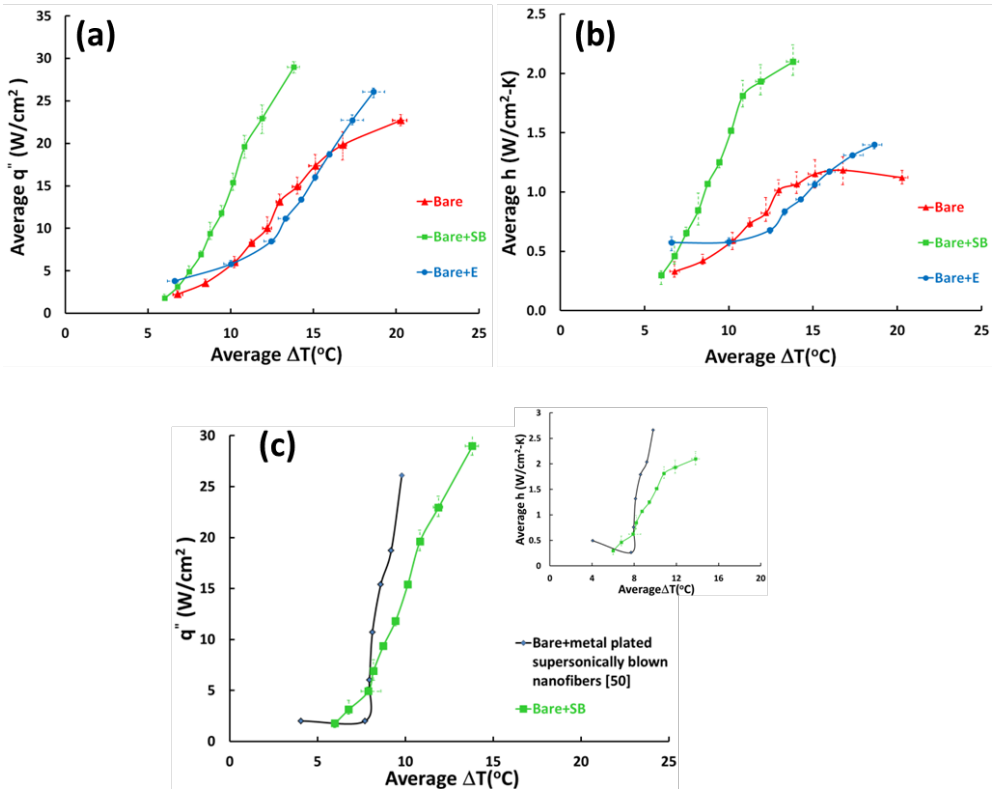


**Fig. 2.** Pool boiling curves for Novec 7300 fluid on Bare, Bare+SB and Bare+E surfaces. The experiments were repeated thrice on the same surface and the average values of q", h

and ΔT are used in these graphs. (a) Heat flux versus surface superheat, and (b) the corresponding heat transfer coefficient versus surface superheat. (c) Boiling curves on Bare+SB surface with polymer nanofibers (from panel a) versus Bare+SB surface with copper-plated nanofibers from [50], with the corresponding heat transfer coefficient versus surface superheat in the inset. The error bars show the maximum and minimum deviations from the average values.

Fig. 3 shows the overall view of the heater surfaces prior and after prolonged boiling. There is no macroscopically visible deterioration of either supersonically-blown nanofibers (Fig. 3b) (which are very thin and look like a milky mat, similarly to [48]), or electrospun nanofibers (Fig. 3c) which are clearly seen. There is also no significant oxidation of the copper surface which would be recognizable by color change.

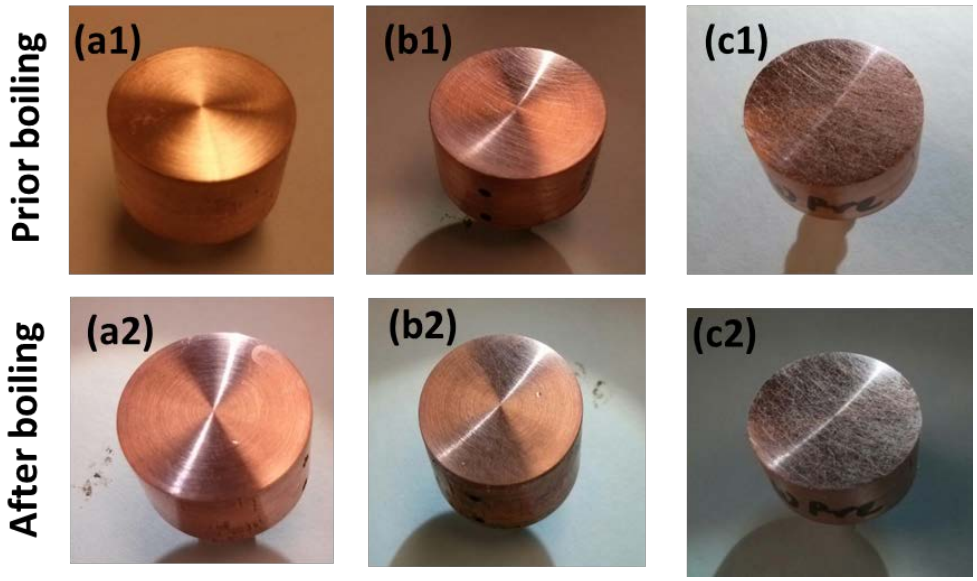


**Fig. 3.** Surface images of the same samples prior (panels with numerals 1) and post boiling (panels with numerals 2) of Novec 7300 fluid for 7.5 h. (a) Bare, (b) Bare+SB

surfaces, (c) Bare+E surfaces. Nanofiber mats are seen as fine white lines on the surfaces, practically invisible on Bare+SB and clearly visible on Bare+E surfaces. The surfaces are 1.9 cm in diameter.

However, the macroscopic images of Fig. 3b-c are insufficient for definite determination of the nanofiber state after prolonged boiling. Therefore, in addition to the macroscopic images of Fig. 3b-c, SEM images of the Bare+SB and Bare+E surfaces are shown in Fig. 4. The latter images reveal that electrospun nanofibers deteriorated in several places and the intact coating ceased to exist after 7.5 h of boiling of Novec 7300. On the other hand, the supersonically-blown nanofibers remained intact after 7.5 h of boiling of Novec 7300.

It should be emphasized that nanofiber adhesion is critical because it results in a better thermal contact of supersonically-blown nanofibers with the heater compared to the electrospun ones. A better thermal contact results in a higher rate of vapor bubble nucleation and removal, and thus intensifies the heat removal process. Additionally, the supersonically-blown nanofibers do not delaminate from the heater due to their stronger adhesion and samples could be used for long multi-hour boiling. The stronger adhesion of the supersonically-blown nanofibers is caused by the van der Waals attraction effective on the scale about 100 nm [52], which is the case of these nanofibers in distinction from the electrospun ones. Accordingly, the superior heat-removal performance of the supersonically-blown nanofiber in comparison with larger electrospun nanofibers stems

from a combination stronger adhesion and faster bubble nucleation on abundant nucleation sites provided by the smaller size nanofibers.

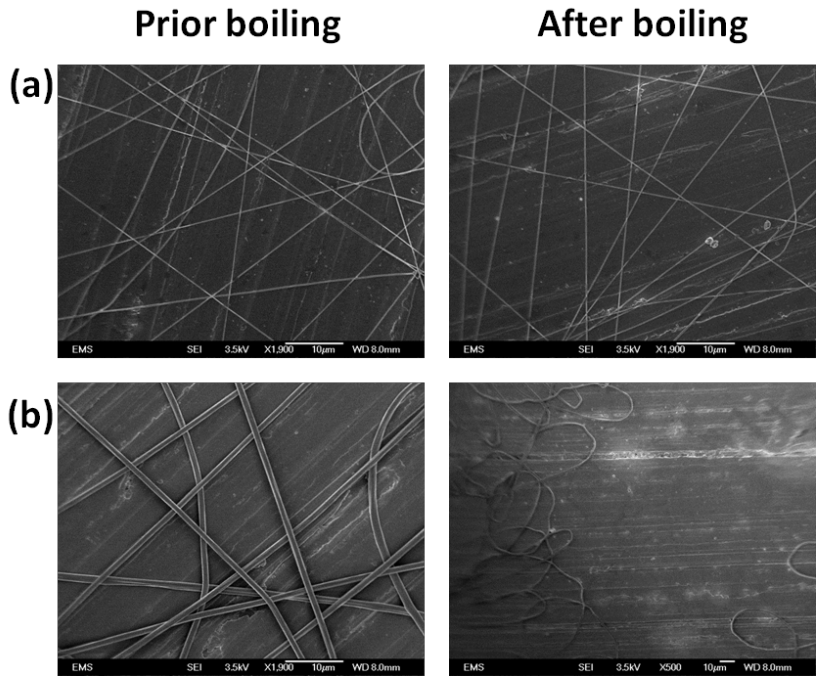


**Fig. 4.** SEM images of the nano-textured surfaces prior and after a prolonged boiling of Novec 7300 for 7.5 h. (a) Bare+SB surface, and (b) Bare+E surface. All scale bars are 10 μm.

The comparison of Figs. 4a and 4b also shows that being observed at the same magnification, supersonically-blown polymer nanofiber mats prior boiling are thinner in comparison to the electrospun ones. Accordingly, the supersonically-blown nanofibers provide much more nucleation sites per unit area than the electrospun ones. The much smaller supersonically-blown polymer nanofibers adhere to the copper substrate much stronger than the electrospun nanofibers.

According to [19], on a surface where active nucleation sites are distributed randomly, the center-to-center distance between the bubbles $S \sim n^{-1/2}$, where n is the surface density of the active nucleation sites. For bare copper surfaces only a few bubbles nucleated from the heater surface itself but rather from its periphery in contact with Teflon [50]. On the other hand, on the copper-plated nanofiber surfaces the entire heater surface contains multiple nucleation sites and generates multiple bubbles [50]. The same phenomenon was observed in the present work (Fig. 5), and since the value of n for solution-blown nanofibers is larger than for the electrospun or bare ones, the former result in a higher heat removal rate. All the surfaces, Bare, Bare+SB and Bare+E, have been compared at same surface superheat of 3.65 $^0$C with only the main cartridge heater supplying heat from the bottom and the immersion heater being off for improved visualization. For the sake of comparison, 114 ms after the onset of boiling of Novec 7300 snapshots of boiling on all the surfaces are shown in Fig. 5 (taken from high-speed videos using Phantom V210 at 2200 fps). It is seen that for Bare+SB surface the bubble density is much higher compared to the bubble density for Bare and Bare+E surfaces.

Careful examination of 80 bubbles on several images using Photoshop revealed the following average bubble radii at the moment of departure from the surface: $0.125 \pm 0.032$ mm for Bare+SB surface, $0.20 \pm 0.044$ mm for Bare+E surface and $0.301 \pm 0.07$ mm for Bare copper surface. In case of the Bare surface the bubble radius r at the departure moment is determined by buoyancy and surface tension, and can be estimated as $r = \left[\sigma / (\rho g)\right]^{1/2}$, with $\rho$ and $\sigma$ being the density and surface tension of liquid and g being gravity acceleration. Taking for the estimate $\rho \sim 1.48$ g/cm$^3$ and $\sigma \sim 10$ g/s$^2$ [53], this expression yields r~0.8 mm, which overestimates the observed value mentioned above.

On the other hand, on nano-textured surfaces, the bubble growth is arrested by the surrounding nanofibers. Fig. 4 shows that the average inter-fiber pore areas on the Bare+SB and the Bare+E surfaces are ~ 30 $\mu m^2$ and 33 $\mu m^2$ with the corresponding porosity of 86% and 78% (Measured using ImageJ software). Accordingly, the pore sizes are of the order of 3 μm, which are significantly smaller than the above-mentioned measured bubble sizes. This corresponds to the observations in [49], where it was argued that vapor jets are squeezed from such pores and undergo the Rayleigh capillary instability which results in bigger bubble formation. Some occasional big bubbles on the Bare+SB surfaces could also be seen, however, most of them originated from the periphery in contact with teflon and were pushed inward. Three high-speed videos of bubble growth and departure from Bare+SB, Bare+E and Bare copper surfaces surfaces are provided as supporting information (SI), where one can see the difference in vapor bubble populations between surfaces. The movies use the images recorded at 2200 fps and reproduced to 30 fps.

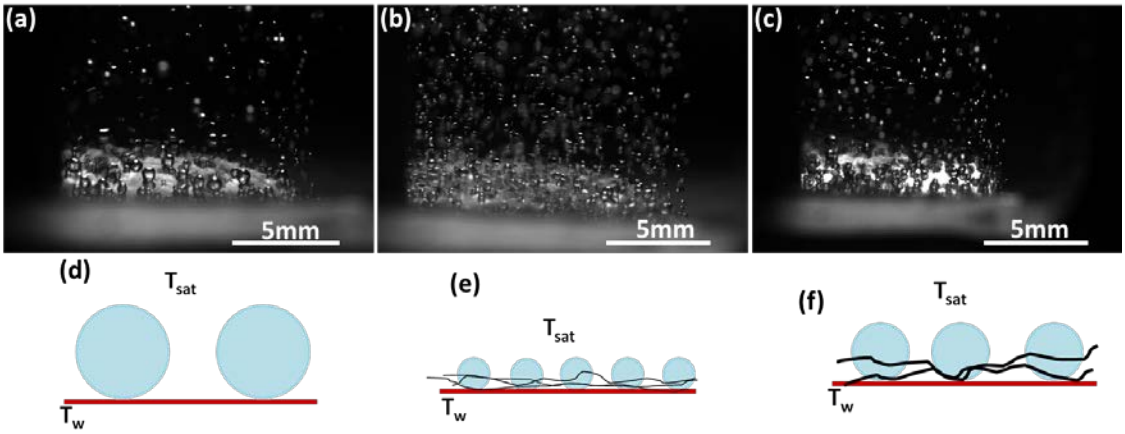

**Fig. 5.** High speed images of vapor bubble nucleation and departure from the heater surface in Novec 7300 fluid. (a) Bare, (b) Bare+SB and (c) Bare+E surfaces. Panels (d), (e) and (f) sketch the phenomena observed in panels (a), (b) and (c), respectively.

It should be emphasized that comparison of Figs. 2a and 2b with Figs. 5a and 5c is quite instructive. Figures 2a and 2b show that the Bare and Bare+E surfaces do perform differently at the beginning of the nucleate boiling, namely the Bare+E surface removes heat at the rate higher by 1.3 W/cm$^2$ than the Bare one at nearly the same surface superheat of about 6.7 ºC. However, the difference diminishes at higher surface superheats and prolonged boiling as the electrospun nanofiber mat begins to deteriorate. The bubble sizes shown in Fig. 5 were measured at the beginning of the boiling cycle when the bubbles are as big as 0.3 mm for the Bare and 0.2 mm for the Bare+E surfaces, respectively. This corresponds to the fact that the Bare+E surface outperforms the Bare surface at this stage, in agreement with the data in Figs. 2a and 2b.

Fewer bubbles nucleating and departing from Bare copper surface generate a weaker convective flow and thus, a diminished heat transfer process compared to that on Bare+SB surface where multiple bubbles appear due to the effect of nanofibers. Correlations for heat flux q" in nucleate pool boiling on bare on horizontal surfaces read [19,54]

$$q'' = c \cdot Pr^{0.33} \cdot k \cdot n^{1/2} \cdot \Delta T \qquad (3)$$

where, q" is the average heat flux (W/cm$^2$), Pr is the Prandtl number, c is a dimensionless constant, k is the thermal conductivity of liquid (W/cm-K), n is the surface density of active nucleation sites (cm$^{-2}$), and $\Delta T$ is the surface superheat (K).

Accordingly, the heat transfer coefficient h (W/cm$^2$-K) is

$$h = c \cdot Pr^{0.33} \cdot k \cdot n^{1/2} \quad (4)$$

The latter equations show that both q" and h increase with the surface density of bubble as $n^{1/2}$ [19, 55]. This conclusion can be extrapolated to the present case of surfaces covered with nanofibers. Also, when the convective flow driven by rising bubbles becomes turbulent [19, 56], the dependence of both q" and h on the Prandtl switches from $Pr^{0.33}$ to $Pr^{0.6}$. For Novec 7300 fluid Pr=21.3, whereas, for DI water Pr=6.41. Therefore, the combined effect of the higher nucleation rate, more frequent bubble departure and faster transition to turbulence in the bubble-driven flow results in the fact that at the same surface superheat both q" and h on the Bare+SB surfaces are larger than those on the Bare+E surfaces, while the latter are larger than the q" and h values for the Bare copper surface.

It should be emphasized that the supersonically-blown PAN nanofibers are very small, of the order of 100 nm in diameter (cf. Fig. 4a), and thus their surface curvature is extremely high. Therefore, they are very effective heat transfer elements to the surrounding medium (liquid in the present case) [57], and thus additionally facilitate nucleate boiling.

### *3.3 Pool Boiling of DI Water*

Experiments conducted with DI water on different substrates were limited to maximum of 60% of the transformer output to avoid reaching CHF. The results are shown in Fig. 6. It is seen that the enhancement of the heat removal rate due to nanofibers at any surface superheat is less pronounced compared to the case of Novec 7300 fluid (Fig. 2), even though the trend stays the same, i.e. the heat transfer is the highest on the Bare+SB surface. The surface superheat of the Bare+SB surface was almost 1.7 $^0$C lower in comparison to that of the bare surface and 1.5 $^0$C lower than that of the Bare+E surface at 60% (the maximum value used) of the total input of the transformer driving the cartridge heater. Note also that the bubble size in pool boiling of DI water was larger than that of Novec 7300 fluid (cf. Fig. 5).

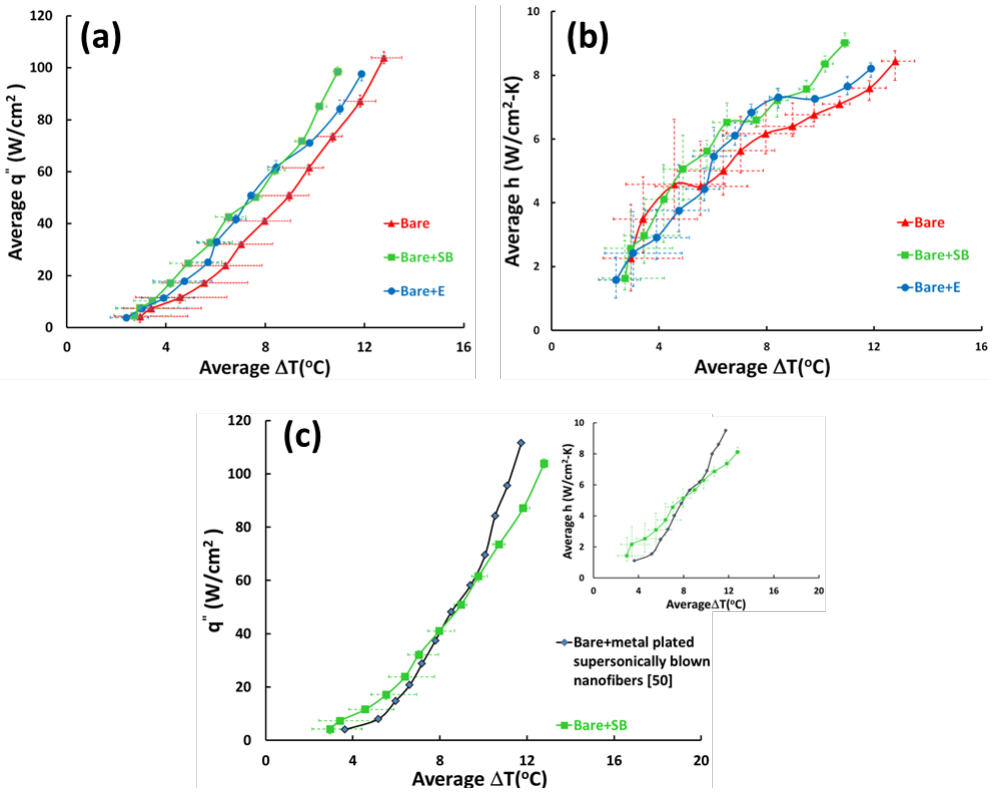


**Fig. 6.** Pool boiling curves for DI water on Bare+SB, Bare, and Bare+E surfaces. The experiments were repeated thrice on the same surface and the average values of q", h and

$\Delta T$ are used in these graphs. (a) Heat flux versus surface superheat, and (b) the corresponding heat transfer coefficient versus surface superheat. (c) Boiling curves on Bare+SB surface with polymer nanofibers (from panel a) versus Bare+SB surface with copper-plated nanofibers from [50], with the corresponding data for the heat transfer coefficient in the inset. The error bars show the maximum and minimum deviations from the average values.

Macroscopic images of test surfaces reveal that boiling of water for several hours on bare Cu surface leads to formation of copper oxide (cf. Fig. 7a), as in [58]. The oxide layer is manifested by green color of the surface. In the case of the Bare copper surface this oxide formation can prevent nucleation and can affect the superheat values in the further trials. The change in the copper surface characteristics due to the formation of the oxide layer is the main reason of the larger data scatter in the case of DI water boiling in comparison to Novec 7300 fluid boiling. In addition, after boiling in DI water on the Bare+E surface the nanofiber layer was completely ripped off (cf. Figs. 7b and 3c2), similarly to some cases reported in [47] for copper-plated nanofibers. This happens mainly due to the growth of vapor bubbles which pull the fibers with forces associated with surface tension, which is high for DI water compared to Novec 7300 fluid. On the contrary, supersonically-blown polymer nanofibers on the Bare+SB samples stayed attached to the substrate surface and mostly retained the architecture of the nanofiber mat. Fig. 7c reveals the presence of a thin white transparent fiber layer on the surface characteristic of the supersonically-blown nanofiber mats, which is confirmed by SEM images in Fig. 8. Fig. 8 shows that the supersonically-blown polymer nanofibers retained

their structures and no delamination from the copper substrate happened. Moreover, these nanofibers seem to be bonded to the copper surface and with each other (cf. Fig. 8b).

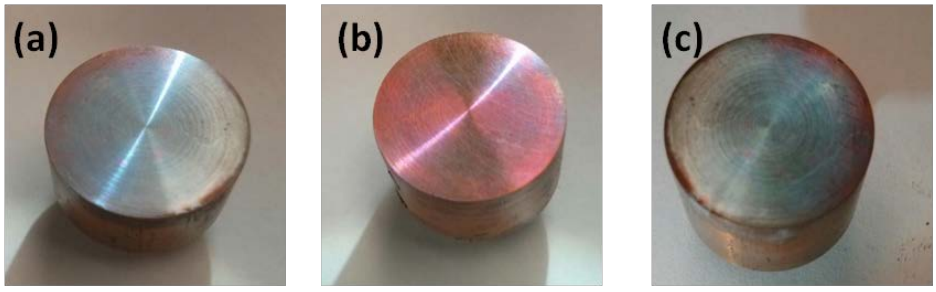


**Fig. 7.** Macroscopic images of the sample surfaces after boiling for 8 hours in DI water. (a) Bare, (b) Bare+SB, and (c) Bare+E surfaces. The green copper oxidized layer on the surfaces is visible. Sample surfaces are of 1.9 cm in diameter.

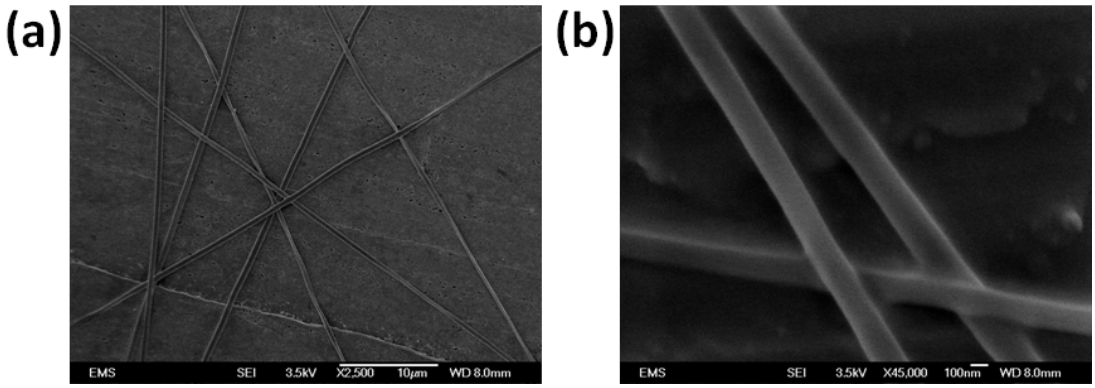


**Fig. 8.** SEM images of the supersonically-blown polymer nanofibers on copper substrate after prolonged boiling for 8 h in DI water. Nanofiber bonding to the surface and to each other is also visible. Scale bar in panel (a) is 10 μm and in panel (b) is 100 nm.

Figs. 2 to 6 show that the effect of supersonically-blown polymer nanofibers on heat transfer to boiling water is less dramatic than for Novec 7300 fluid. Figs. 4, 7 and 8

also show that supersonically solution-blown nanofibers slightly changed morphology after boiling in water being sintered to each other, whereas boiling in Novec 7300 fluid no morphology changes have been observed. Smaller bubbles in Novec 7300 fluid intensify the heat removal rate in it in comparison to the bare surface more effectively than in water boiling in comparison to bare surface was not drastic. That is probably the reason of the inter-polymer fiber bonding in boiling water, given the fact that PAN nanofibers have the glass transition temperature around 100 $^0$C (the boiling point of water), which should not be confused with melting, since melting point of PAN is nearly 320 $^0$C. Note also that up to $\Delta T \sim 9$ $^0$C the supersonically-blown polymer nanofiber mat performed better than the supersonically-blown metal-plated nanofiber mat (cf. Fig. 6c).

## 4. Conclusion

Pool boiling experiments with Novec 7300 and water conducted on bare Cu surface, and copper surface coated with either electrospun or supersonically-blown polymer nanofibers revealed significant benefits of the latter. Namely, the supersonically-blown polymer nanofibers significantly enhanced the heat removal rate from the heater surface, especially in the case of Novec 7300 fluid where the maximum surface superheat was reduced by at least 7 $^0$C versus 5 $^0$C for the electrospun surface. The supersonically-blown 100 nm polymer nanofibers facilitated bubble nucleation serving as active nucleation sites. Such nanofiber mats also possess a larger number of small pores than electrospun nanofibers, which cut and release the growing bubbles. Supersonically-blown nanofibers revealed the best adhesion to the copper substrate and

retained their architecture after prolonged 7.5 h of boiling. The experiments conducted with DI water did not show as strong enhancement of the heat removal rate, as the experiments with Novec 7300 fluid did, even though compared to the bare copper surface, the surface superheat was reduced on supersonically-blown nanofibers by ~1.7 $^0$C at the maximum heat flux after 8 h of boiling. Novec 7300 is a low surface tension fluid and the onset of heterogeneous nucleate boiling takes place at a lower surface temperature compared to DI water. Accordingly, in Novec 7300 fluid the size of vapor bubbles is smaller and thus affected by the nano-texture of the heater surface. DI water, on the other hand, possesses a high surface tension, and thus the onset of boiling takes place at a higher surface temperature. The larger bubbles in DI water are insignificantly affected by the surface nano-texture, and accordingly, the enhancement of heat removal is diminished in DI water compared to Novec 7300 fluid. Note also that after boiling in DI water, electrospun nanofibers were completely delaminated from the copper substrate, unlike the supersonically-blown nanofibers which retained their adhesion and architecture. The inexpensive surfaces coated with supersonically-blown nanofibers can remove heat at the rate of ~30 W/cm$^2$ in Novec 7300 fluid.

**Achnowledgement**

This work is supported by NASA (Grant No. NNX13AQ77G).

**References**

1. Q. Guo, L. M. Keer and Y.W. Chung, Thermal Stress-Induced Open-Circuit Failure in Microelectronics Thin-Film Metallizations (Chapter 10) (Editor: John H. Lau), Thermal Stress and Strain in Microelectronics Packaging, 1993, Springer-Verlag.
2. A. Miner and U. Ghoshal, Limits of Heat Removal in Microelectronic Systems, IEEE Transactions on Components and Packaging Technologies, 2006, 29, 743-749.
3. H. Y. Zhanga, D. Pinjalaa, T.N. Wongb, K.C. Tohb and Y.K. Joshic, Single-Phase Liquid Cooled Microchannel Heat Sink for Electronic Packages, Applied Thermal Engineering, 2005, 25, 1472–1487.
4. X. F. Peng, G. P. Peterson and B. X. Wang, Frictional Flow Characteristics of Water Flowing Through Microchannels, Experimental Heat Transfer, 1994, 7, 249–264.
5. X. F. Peng, G. P. Peterson and B. X. Wang, Heat Transfer Characteristics of Water Flowing through Microchannels, Experimental Heat Transfer, 1994, 7, 265–283.
6. L. P. Yarin, A. Mosyak and G. Hetsroni, Fluid Flow, Heat Transfer and Boiling in Micro-Channels, Springer, Berlin, 2009.
7. H. L. Souza Lara Leão, F. J. do Nascimento and Gherhardt Ribatski, Flow Boiling Heat Transfer Of R407C in a Microchannels Based Heat Spreader, Experimental Thermal and Fluid Science, 2014, 59, 140–151.
8. N. Beratlis and M. Smith, Optimization of Synthetic Jet Cooling for Micro-electronics Applications, Proceedings of 19th Semi-Therm Symposium, San Jose, CA, 2003, 66-73.
9. E. N. Wang, L. Zhang , L. Jiang, Jae-Mo Koo, J. G. Maveety , E. A. Sanchez, K. E. Goodson and T. W. Kenny, Micromachined Jets for Liquid Impingement Cooling of

VLSI Chips, Micromachined Jets for Liquid Impingement Cooling of VLSI Chips**,** Journal of Microelectromechanical Systems, 2004, 13, 833 – 842.

10. S. An, C. Lee, M. Liou, H. S. Jo, J.-J. Park, A. L. Yarin and S. S. Yoon. Supersonically Blown Ultra-thin Thorny Devil Nanofibers for Efficient Air Cooling. ACS Applied Materials & Interfaces, 2014, 6, 13657-13666.
11. A. C. Cotler, E. R. Brown, V. Dhir and M. C. Shaw, Chip-Level Spray Cooling of an LD-MOSFET RF Power Amplifier, IEEE Transactions on Components and Packaging Technologies, 2004, 27, 411-416.
12. J. Kim and E. Golliher, Steady State Model of a Micro Loop Heat Pipe, Proceedings of 18th Semi-Therm Symposium, San Jose, CA, 2002, 137-144.
13. I. Silverman, A.L. Yarin, S.N. Reznik, A. Arenshtam, D. Kijet and A. Nagler, High Heat-flux Accelerator Targets: Cooling with Liquid Metal Jet Impingement, Int. J. Heat and Mass Transf., 2006, 49, 2782-2792.
14. A. Miner, U. Ghoshal, Cooling of High-Power-Density Microdevices Using Liquid Metal Coolants, Applied Physics Letters, 2004, 85, 506–508.
15. S. Sinha-Ray, S. Sinha-Ray, H. Sriram and A. L. Yarin, Flow of Suspensions of Carbon Nanotubes Carrying Phase Change Materials Through Microchannels and Heat Transfer Enhancement, Lab Chip, 2014, 14, 494-508.
16. T. M. Anderson and I. Mudawar, Microelectronic Cooling by Enhanced Pool Boiling of a Dielectric Fluorocarbon Liquid, Journal of Heat Transfer, 1989, 111, 752-759.
17. R. L. Webb and N. H. Kim, Principles of Enhanced Heat Transfer, Second Ed., Taylor & Francis, New York, 2005, 389-391
18. S. S. Kutateladze, Fundamentals of Heat Transfer, 1963, Academic Press, New York.

19. C. L. Tien, A Hydrodynamic Model for Nucleate Pool Boiling, International Journal of Heat and Mass Transfer, 1962, 5, 533-540.
20. S. Nukiyama, The Maximum And Minimum Values of The Heat Q Transmitted From Metal to Boiling Water Under Atmospheric Pressure, International Journal of Heat and Mass Transfer, 1966, 9, 1419-1433.
21. R. Rioboo, M. Marengo, S. Dall'Olio, M. Voué and J. De Coninck, An Innovative Method to Control The Incipient Flow Boiling Through Grafted Surfaces With Chemical Patterns, Langmuir, 2009, 25, 6005-6009.
22. L. Dong, X. Quan and P. Cheng, An Experimental Investigation of Enhanced Pool Boiling Heat Transfer From Surfaces With Micro/Nano-Structures, International Journal of Heat and Mass Transfer, 2014, 71, 189-196.
23. C. Li and G.P. Peterson, Geometric Effects on Critical Heat Flux on Horizontal Microporous Coatings, Journal of Thermophysics Heat Transfer, 2010, 24, 449-455.
24. K. N. Rainey and S.M. You, Pool Boiling Heat Transfer From Plain and Microporous, Square Pin-Finned Surfaces In Saturated FC-72, Journal of Heat Transfer, 2000, 122, 509-516.
25. J. P. McHale, S. V. Garimella, T. S. Fisher and G. A. Powell. Pool Boiling Performance Comparison af Smooth And Sintered Copper Surfaces With and Without Carbon Nanotubes, Nanoscale and Microscale Thermophysical Engineering, 2011, 15, 133-150.
26. J. Y. Chang and S. M. You, Boiling Heat Transfer Phenomena From Microporous and Porous Surfaces in Saturated FC-72, International Journal of Heat and Mass Transfer, 1997, 40, 4437-4447.

27. S. J. Kim, I.C. Bang, J. Buongiorno and L.W. Hu, Surface Wettability Change During Pool Boiling of Nanofluids and Its Effect on Critical Heat Flux. International Journal of Heat and Mass Transfer, 2007, 50, 4105-4116.
28. Y. Y. Li, Z. H. Liu and B. C. Zheng, Experimental Study On The Saturated Pool Boiling Heat Transfer on Nano-Scale Modification Surface, International Journal of Heat and Mass Transfer, 2015, 84, 550-561.
29. B. Bourdon, P. Di Marco, R. Rioboo, M. Marengo and J. De Coninck, Enhancing The Onset of Pool Boiling by Wettability Modification on Nanometrically Smooth Surfaces, International Communication of Heat and Mass Transfer, 2013, 45, 11-15.
30. R. Rioboo, M. Marengo, S. Dall'Olio, M. Voué and J. De Coninck, An Innovative Method to Control The Incipient Flow Boiling Through Grafted Surfaces With Chemical Patterns, Langmuir, 2009, 25, 6005-6009.
31. W.F. Calus and D.J. Leonidopoulos, Pool Boiling- Binary Liquid Mixtures, International Journal of Heat and Mass Transfer, 1974, 17, 249-256.
32. M. K. Jensen and D. L. Jackman, Prediction of Nucleate Pool Boiling Heat Transfer Coefficients of Refrigerant-Oil Mixtures, Journal of Heat Transfer, 1984, 106, 184-190.
33. Z. Sun, M. Gon, Y. Qi, Z. Li and J. Wu, Nucleate Pool Boiling Heat Transfer of Pure Refrigerants and Binary Mixtures, Journal of Thermal Science, 2004, 13, 259-263.
34. W. R. Mcgillis and V.P. Carey, On the Role of Marangoni Effects on the Critical Heat Flux for Pool Boiling of Binary Mixtures, Journal of Heat Transfer, 1196, 118, 103-109.
35. A. Sathyanarayana, P. Warrier, Y. Im, Y. Joshi and A. S. Teja, Pool Boiling of HFE 7200–C4H4F6O Mixture on Hybrid Micro-Nanostructured Surface, Journal of Nanotechnology in Engineering and Medicine. 2012, 3, 041004.

36. E. C. Forrest, L. W. Hu, J. Buongiorno and T.J. McKrell, Pool Boiling Heat Transfer Performance of A Dielectric Fluid With Low Global Warming Potential. Heat Transfer Engineering, 2013, 34, 1262-1277.
37. M. Amaya, S. M. Kwark, A. Gurung and S. M. You, Pool boiling heat transfer of borated ($H_3BO_3$) Water on a nanoporous surface, Journal of Heat Transfer, 2013, 135, 091302.
38. H. Kim, M. Kim, Experimental Study of The Characteristics and Mechanism of Pool Boiling CHF Enhancement Using Nanofluids, Heat and Mass Transfer, 2009, 45, 991-998.
39. D. Wen and Y. Dong, Experimental Investigation Into The Pool Boiling Heat Transfer of Aqueous Based γ-Alumina Nanofluids, Journal of Nanoparticle Research, 2005, 7, 265-274.
40. S. K. Das, N. Putra, W. Roetzel, Pool Boiling Characteristics of Nano-Fluids, International Journal of Heat and Mass Transfer, 2003, 46, 851-862.
41. S. M. You, J. H. Kim and K. H. Kim, Effect of Nanoparticles on Critical Heat Flux of Water in Pool Boiling Heat Transfer, Applied Physics Letters, 2003, 83, 3374-3376.
42. G. Quinn and B. M. Cetegen, Effect of Surfactant Addition on Boiling Heat Transfer on a Liquid Film Flowing in a Diverging Open Channel, International Journal of Heat and Mass Transfer, 2010, 53, 245–253.
43. C. M. Weickgenannt, Y. Zhang, S. Sinha-Ray, I. V Roisman, T. Gambaryan-Roisman, C. Tropea and A. L. Yarin, Inverse-Leidenfrost Phenomenon on Nanofiber Mats on Hot Surfaces, Physical Review E, 2011, 84, 036310.

44. S. Sinha-Ray, Y. Zhang and A.L. Yarin, Thorny Devil Nanotextured Fibers: The Way to Cooling Rates on The Order of 1 Kw/cm2. Langmuir, 2010, 27, 215-226.
45. S. Sinha-Ray and A. L. Yarin, Drop Impact Cooling Enhancement on Nano-Textured Surfaces. Part I: Theory and Results of the Ground (1g) Experiments, International Journal of Heat and Mass Transfer, 2014, 70, 1095-1106.
46. S. Sinha-Ray, S. Sinha-Ray, A. L. Yarin, C. M. Weickgenannt, J. Emmert and C. Tropea, Drop Impact Cooling Enhancement on Nano-Textured Surfaces. Part II: Results of the Parabolic Flight Experiments [Zero Gravity (0 g) And Supergravity (1.8 g)], International Journal of Heat and Mass Transfer, 2014, 70, 1107-1114.
47. S. Jun, S. Sinha-Ray and A. L. Yarin. Pool Boiling on Nano-textured Surfaces, International Journal of Heat and Mass Transfer, 2013, 62, 99-111.
48. S. Sinha-Ray, M. W. Lee, S. Sinha-Ray, S. An, B. Pourdeyhimi, S. S. Yoon and A. L. Yarin, Supersonic Nanoblowing: A New Ultra-Stiff Phase of Nylon 6 in 20–50 nm Confinement, Journal of Material Chemistry C, 2013, 1, 3491–3498.
49. R. P. Sahu, S. Sinha-Ray, S. Sinha-Ray and A. L. Yarin, Pool Boiling on Nano-Textured Surfaces Comprised of Electrically-Assisted Supersonically Solution-Blown, Copper-Plated Nanofibers: Experiments and Theory, International Journal of Heat and Mass Transfer, 2015, 87, 521-535.
50. R. P. Sahu, S, Sinha-Ray, S. Sinha-Ray and A. L Yarin, Pool Boiling of Novec 7300 and Self-Rewetting Fluids on Electrically-Assisted Supersonically Solution-Blown, Copper-Plated Nanofibers International Journal of Heat and Mass Transfer, 2016, 95, 83-93

51. M. Freysteina, F. Kolberg, L. Spiegel, S. Sinha-Ray, R. P. Sahu, A. L. Yarin, T. Gambaryan-Roisman and P.Stephan, Trains of Taylor Bubbles Over Hot Nano-Textured Mini-Channel Surface, International Journal of Heat and Mass Transfer, 2016, 93, 827–833.
52. S. Sinha-Ray, S. Sinha-Ray, B. Pourdeyhimi, A.L. Yarin. Application of Solution-blown 20-50 nm Nanofibers in Filtration of Nanoparticles: The Efficient van der Waals Collectors, J. Membrane Sci. 2015, 485, 132-150.
53. http://multimedia.3m.com/mws/media/338713O/3mtm-novectm-7300-engineered-fluid.pdf
54. K. Nishikawa and K. Yamagata, On the Correlation of Nucleate Boiling Heat Transfer, International Journal of Heat and Mass Transfer, 1960, 1, 219-235.
55. R. F. Gaertner and J. W. Westwater, Population of active Sites in Nucleate Boiling Heat Transfer, Chemical Engineering Program Symposium, 1960, 30, 39-48.
56. N. Zuber, Nucleate Boiling: The Region of Isolated Bubbles and The Similarity With Natural Convection, International Journal of Heat and Mass Transfer, 1961, 6, 53-78.
57. Ya. B. Zeldovich, G. I.Barenblatt, V. B. Librovich and G. M. Makhviladze, The Mathematical Theory of Combustion and Explosions. Consultants Bureau, New York, 1985.
58. M. Moliere, Y. Verdier and C. Leymonie, Oxidation of Copper on High Purity Water at 70°C: Application to Electric Generator Operation, Corrosion Science, 1990, 30, 183-188.